https://doi.org/10.22226/2410-3535-2023-1-50-55

Optical and dielectric properties of nanosized ceramics $Bi_2Mg_{1-x}Cr_xTa_2O_{9.5-\Delta}$ with pyrochlore structure

E. A. Serebryakov[†,1], A. D. Shpynova[1], R. I. Korolev[1], N. A. Sekushin[2], A. A. Selyutin[3], B. A. Makeev[4], N. A. Zhuk[1]

[†]gabdraufmanhik@gmail.com

[1]Syktyvkar State University, Syktyvkar, 167001, Russia
[2]Institute of Chemistry of the Komi Science Center UB RAS, Syktyvkar, 167982, Russia
[3]Saint Petersburg State University, St. Petersburg, 199034, Russia
[4]Institute of Geology of the Komi Science Center UB RAS, Syktyvkar, 167982, Russia

Chromium-containing pyrochlores $Bi_2Mg_{1-x}Cr_xTa_2O_{9.5-\Delta}$ with a variable content of magnesium/chromium ions were obtained by solid-phase synthesis. The synthesized samples were characterized by a loose nanosized microstructure formed by partially intergrown ceramic grains. They were bright green. With an increase in the chromium content in the samples, the unit cell parameter of the solid solutions decreased from 10.4890 to 10.4467 Å, obeying Vegard's rule. The absorption spectra of chromium pyrochlores contained several features in the range below 400 nm, a shoulder in the range of 450 – 520 nm, a broad absorption in the range of 600 – 700 nm with a maximum at 650 nm, and a narrow peak at 724 nm. The band gap of the obtained materials for direct allowed most intense electronic transitions was in the range of 2.14 – 2.29 eV. At 23°C, the permittivity of the samples in a wide frequency range (10^2 – 10^6 Hz) was practically independent of frequency and decreased with increasing content of chromium ions in solid solutions from 19.5 to 16.5 at 10^6 Hz. Above 10^5 Hz, the dielectric loss tangent for all samples slightly depended on frequency and took low values of 0.004 (10^6 Hz). The conduction activation energy for the samples varied in the range 1.39 ÷ 1.48 eV.

Keywords: pyrochlore, CrMg codoping, band gap, diffuse reflection spectra, dielectric properties.

1. Introduction

Synthetic pyrochlores attract close attention of scientists due to the manifestation of practically useful physicochemical properties, such as proton conductivity, excellent photocatalytic and dielectric properties [1–4]. The flexibility of the crystal structure of pyrochlores to cation substitutions and vacancies in the anion sublattice makes it possible to significantly vary the chemical composition of compounds and obtain hundreds of combinations of compositions with various functional properties. Oxide pyrochlores are described by the general formula $A_2B_2O_6O'$ with a combination of three- and four- ($A^{3+}{}_2B^{4+}{}_2O_7$) or di- and pentavalent elements ($A^{2+}{}_2B^{5+}{}_2O_7$) in the cation sublattices A and B [5,6]. The B_2O_6 cationic sublattice is formed by [BO_6] octahedra connected at the corner vertex. The A_2O' sublattice has an anticristobalite structure formed by [$O'A_4$] tetrahedra. Relatively small cations (Ti^{4+}, Ta^{5+}, Sb^{5+}, Nb^{5+}) occupy the B cationic positions, while large A ions (Ca^{2+}, Bi^{3+}, Pb^{2+}) are located in the eight-vertex formed by the oxygen atoms of the A_2O' and B_2O_6 sublattices [7–9]. Mixed bismuth-containing pyrochlores are known ($A^{3+}{}_2M^{2+}B^{5+}{}_2O_9 = A^{3+}{}_{4/3\square 2/3}M^{2+}{}_{2/3}B^{5+}{}_{4/3}O_{6\square 1}$, where □ — vacancies), the crystal framework of which is formed by tri- and pentavalent elements and is stabilized introduction of divalent or trivalent cations M (M-Mg, 3d-elements), commensurate with the B ion [10–13]. In this case, the cationic sublattice B is filled, and the anionic and cationic sublattices A are ideally 14 and 33 percent vacant, respectively. The sublattice of cations A always remains partially vacant, probably due to the influence of the stereoactive $6s^2$ electron pair of bismuth (III) ions. Mixed bismuth-containing pyrochlores are promising as proton conductors and exhibit good dielectric properties [14,15]. Most pyrochlores based on bismuth tantalate are characterized by a nanosized microstructure formed during the ceramic synthesis method and are promising as photocatalysts. A large number of works are aimed at searching for new representatives of this group of compounds. At present, iron- [11,16], copper- [17,18], nickel- [10], magnesium- [12], zinc- [19], cobalt-containing [13] pyrochlores based on bismuth tantalate have been studied in detail. Few works are available on manganese- and chromium-containing pyrochlores. One work on chromium pyrochlore is known [20], in which the structure of the $Bi_{2-x}(CrTa)O_{7-y}$ compound was studied in detail according to neutron and synchrotron X-ray data. In this article, we report on the study of the optical and electrical properties of a new series of chromium and magnesium-containing $Bi_2Mg_{1-x}Cr_xTa_2O_{9.5-\Delta}$ solid solutions based on bismuth tantalate with a pyrochlore structure.

2. Experimental

Solid solutions $Bi_2Mg_{1-x}Cr_xTa_2O_{9.5-\Delta}$ ($x = 0.3, 0.5, 0.7$) were synthesized by the solid-phase method. Ceramic synthesis took place in 4 stages, at a temperature of 650, 850,950,1050°C for 15 hours at each stage of calcination. Bi_2O_3, MgO, Cr_2O_3, and Ta_2O_5 oxides served as precursors for the solid-phase reaction. Scanning electron microscopy and energy dispersive X-ray spectroscopy (electron scanning microscope Tescan VEGA 3LMN, energy dispersion spectrometer INCA Energy 450) were used to study the microstructure and local elemental composition of the samples. The formation of single pyrochlore phases was confirmed by X-ray diffraction (XRD) analysis using a Shimadzu 6000 instrument (CuK_α radiation, $2\theta = 10 - 70°$, scan rate of 2°/min). In order to study electrical properties, metallic Ag electrodes were applied onto both sides of the ceramic discs and sintered at 650°C for 1 h. The measurements were carried out with an E7-28 impedancemeter (frequency range of $25 - 10^7$ Hz) at temperatures from 25 up to 450°C. The thickness and diameter of the studied disk-shaped sample were 2.0 – 2.3 and 14.2 mm, respectively. Diffuse reflectance spectra were recorded in the range of 200 – 900 nm using a Shimadzu UV-2550 spectrophotometer with a spectral step of 1 nm. Halogen and deuterium lamps were used as the radiation source. The spectra were obtained for substances in a barium sulfate matrix. The scattering spectrum from the pure barium sulfate matrix was subtracted from the resulting spectrum. For a quantitative description of the diffuse scattering spectra, the basis of the Kubelka-Munk theory was applied. The value of E_g was determined by the position of the fundamental absorption edge according to the Tauc equation $(h\nu F(r))1/n = A(h\nu - E_g)$, where E_g is the band gap, h is Planck's constant, ν is the oscillation frequency of electromagnetic waves, $F(r) = (1-r)^2/2r$ is the Kubelka-Munk function, A is a constant. The exponent value for direct allowed transitions is $n = 1/2$. The diffuse scattering spectra were rearranged in Tauc coordinates: $(h\nu F(r))^2$ versus E (eV). The E_g value was determined by extrapolating the linear section of the Tauc curve to the energy axis.

3. Results and discussion.

Based on X-ray phase analysis, it was found that the $Bi_2Mg_{1-x}Cr_xTa_2O_{9.5-\Delta}$ ($x = 0.3, 0.5, 0.7$) samples crystallize in the cubic system. An analysis of reflection extinctions showed that the symmetry of the crystal structure is cubic, belonging to the space group *Fd*-3*m*.

With an increase in the content of chromium ions in the samples, the unit cell parameter decreases from 10.4890(8) Å ($x = 0.3$), 10.4669(8) ($x = 0.5$) to 10.4467(7) Å ($x = 0.7$) obeying Vegard's rule (Fig. 1). This fact may indicate the formation of a continuous series of solid solutions and the predominant distribution of chromium and magnesium ions in one system of crystallographic positions. The decrease in the cell constant is associated with a decrease in the content of magnesium (II) cations in solid solutions, the ionic radius of which is larger than that of tantalum (V) and Cr(III) ions, but smaller than that of bismuth (III) ($R(Mg^{2+})_{c.n.-6} = 0.72$ Å, $R(Ta^{5+})_{c.n.-6} = 0.64$ Å, $R(Cr^{3+})_{c.n.-6} = 0.615$ Å, $R(Bi^{3+})_{c.n.-8} = 1.17$ Å, $R(Mg^{2+})_{c.n.-8} = 0.89$ Å) [21]. The presence of chromium (III) ions in the samples is indisputable, since the samples have a characteristic green color, the intensity of which increases with increasing chromium content in the samples. The calculated unit cell parameters of solid solutions are comparable with the values given in the article [20] for chromium-containing pyrochlore $Bi_2(CrTa)O_7$ ($a = 10.451$ Å).

We believe that it is impossible to exclude the presence in solid solutions of oxidized Cr(VI) ions, the ionic radius of which is smaller than the ionic radius of Ta (V) ($R(Ta^{5+})_{c.n.-6} = 0.64$ Å, $R(Cr^{6+})_{c.n.-6} = 0.44$ Å). The presence of Cr (VI) ions in ceramics was noted earlier in solid solutions based on bismuth niobates $BiNbO_4$, $Bi_5Nb_3O_{15}$ and detected by magnetic dilutionx [22, 23]. Since the radius of Cr(III) and Cr(VI) ions is small compared to bismuth (III) ions, it is advantageous for chromium ions to occupy the octahedral positions of tantalum.

The microstructure of the samples is porous, reticular, formed by weakly aggregated elongated particles (Fig. S1, supplementary material). No significant dependence of the crystallite size on the magnesium/chromium ratio has been established. The average size of crystallites determined by the Scherrer method for solid solutions is ≈0.064 μm, meanwhile, larger grains with a longitudinal size of 0.5 – 2 μm were recorded by scanning electron microscopy (SEM). In some places, local coalescence of grains with the formation of larger aggregates is observed. As the EDS analysis showed, the experimental composition of the samples satisfies the target compositions (Fig. S2, supplementary material).

Diffuse reflectance spectra of samples of solid solutions $Bi_2Mg_{1-x}Fe_xTa_2O_{9+\Delta}$ ($x = 0.3$ and 0.7) are shown in Fig. 2.

The band gap (E_g) of chromium-containing pyrochlores for direct allowed electronic transitions was estimated from the data of the diffuse reflection spectrum (Fig. 3) for samples with different chromium content $x = 0.3$ and $x = 0.7$. As the figure shows, both samples have a significant reflection in the green (552 and 558 nm) region. A weak reflex is observed in the red (710 nm) range. Apparently, the reflection in the green range of the visible color is associated with the color of the samples of emerald green. We assume that the reflection at 710 nm can be associated with the presence of a small

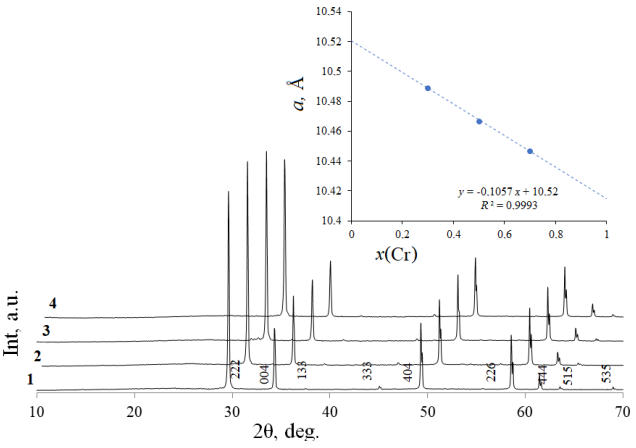

Fig. 1. XRD patterns of $Bi_2Mg_{1-x}Cr_xTa_2O_{9.5-\Delta}$ ($x = 0.3, 0.5, 0.7$) and the dependence of the unit cell parameter on the content of chromium ions in solid solutions.

amount of chromium (VI) ions. From considerations of the electronic balance, it is advantageous for the system to have Cr(VI) ions compared to Cr(III), in this case, the tension of the pyrochlore structure due to oxygen vacancies decreases due to the heterovalent substitution of Nb(V) ions by chromium ions. In addition, the presence of chromium (VI) ions was detected by magnetic dilution in solid solutions of heterovalent substitution of bismuth niobates [22,23]. Calculations showed that the band gap for direct allowed transitions in x(Cr) = 0.3 and 0.7 samples is 1.52 and 1.58 eV and 2.29 and 2.14 eV, respectively. These energy values correspond to absorption at 822 and 790 nm and 545 and 583 nm from chromium (VI) and (III) ions, respectively. In this case, with an increase in the chromium content in the samples, the band gap increases and the energy gap between the valence band and the conduction band increases. It can be stated that doping with chromium reduces the photoactivity of pyrochlore. Meanwhile, the band gap of the studied ceramics is close to the energy of solar radiation reaching the surface of our planet and having a maximum intensity (2.1–2.5 eV). This causes the prospect of using these materials as light-absorbing elements for solar cells. $Bi_2Mg_{0.5}Cr_{0.5}Ta_2O_{9.5-\Delta}$.

For the samples of solid solutions $Bi_2Mg_{1-x}Cr_xTa_2O_{9.5-\Delta}$ (x = 0.7, 0.5, 0.3) at room temperature, the electrical characteristics were studied — the permittivity and dielectric loss tangent in the frequency range 25 Hz–10 MHz (Fig. 3) depending on on the magnesium/chromium ratio.

Measurements of the electrical properties at room temperature showed that the permittivity of the samples in a wide frequency range (10^2–10^6 Hz) is practically independent of frequency and exhibits low values ε ≈ 16.5–19.5 (10^6 Hz). In the low-frequency range, the dielectric constant for all frequencies increases by 1–2 units, reaching for x = 0.3 values over 20.5 at 25 Hz. A weak concentration dependence is observed (with an increase in the x index by 0.4 (more than twice), the permittivity ε decreases by 3 units), according to which, with an increase in the chromium content (and a decrease in magnesium) in the samples, the dielectric permittivity decreases. The smallest values of dielectric permittivity characterize the sample for which x(Cr) = 0.7 maximum. The presence of a concentration regularity is indicated by the sequence of dependences of ε on the x index. Considering that when magnesium (II) ions are replaced by chromium (III) ions, the total atomic polarizability in the samples increases (α(Mg(II) = 1.32 Å^3, α(Cr(III) = 1.45 Å^3), one would expect a slight increase in the permittivity with increasing chromium concentration, which did not happen. We assume that the microstructure of the ceramic may be the reason for this, as well as the tendency of the samples to absorb water. Assuming that the microstructure of the ceramic, in particular the grain size or the area of grain boundaries, is the main cause. of many individual grains is characterized by a significant grain boundary area Grain boundary regions can have an increased content of cationic defects or oxygen vacancies, which increases the grain boundary conductivity, causing a decrease in the difference between the ceramic grain resistance and the grain boundary resistance In general, this leads to less polarization on the grain, which leads to low

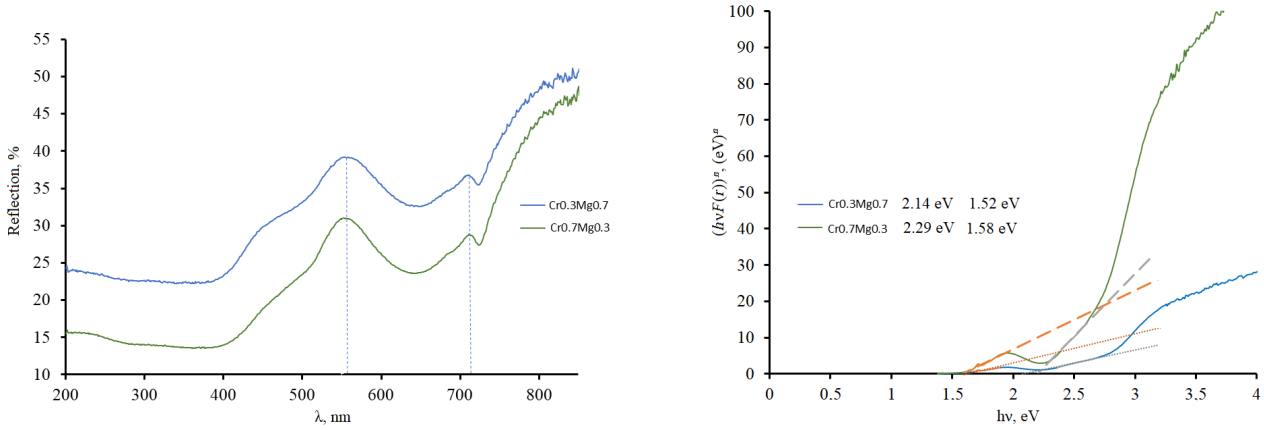

Fig. 2. Diffuse reflectance spectra of the $Bi_2Mg_xFe_{1-x}Ta_2O_{9.5-\Delta}$ samples and Tauc curves for samples and their corresponding energies of direct allowed transitions.

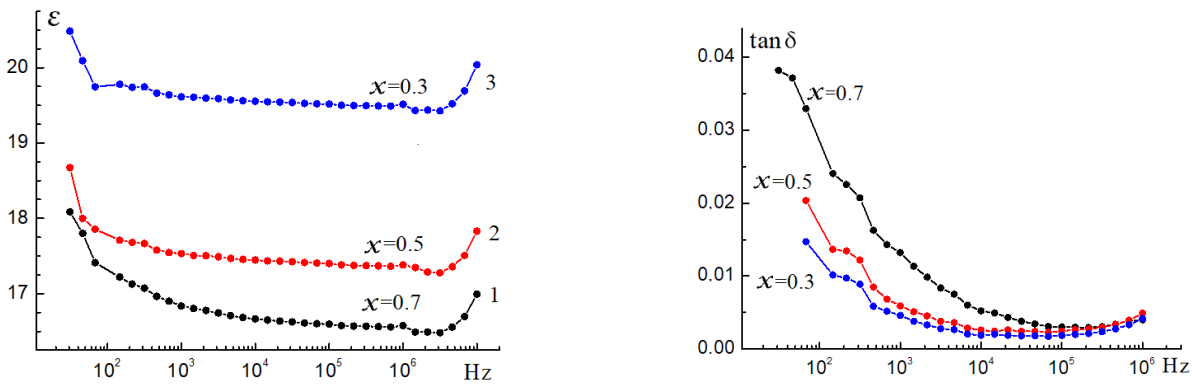

Fig. 3. (Color online) Dielectric permittivity and dielectric loss tangent of $Bi_2Mg_{1-x}Cr_xTa_2O_{9.5-\Delta}$ samples at x = 0.7(1), 0.5(2), 0.3(3) at 23°C.

values of the permittivity., with an increase in the chromium content, the grain size decreases. This conclusion confirms the increased dielectric loss tangent for sample number 1 ($x = 0.7$). The dielectric loss tangent exhibits a similar course of dependence for all samples. Above 10^5 Hz, the loss tangent for all samples is slightly dependent on frequency and takes low values of 0.004 (10^6 Hz). For $Bi_2MgTa_2O_9$ [24] at room temperature and a frequency of 1 MHz, the permittivity and dielectric loss tangent are 20 and $2 \cdot 10^{-3}$, respectively. It should be noted the almost exact coincidence of the values and the reproducibility of the properties of preparations from different series and prepared at different times. It is interesting to emphasize that the permittivity of Fe, Mg-codoped bismuth tantalate is one and a half times higher than for magnesium-containing pyrochlores of the same composition. The permittivity of Fe, Mg-codoped bismuth tantalate also depends on the magnesium/iron ratio and takes on the higher values, the more iron (III) ions in the samples are 28.5 – 30.5 and 0.001 (1 MHz).

For samples stored in air, we observed an extremum in the temperature dependence of the permittivity at frequencies below 3.2 kHz (Fig. 4). The maximum of different intensity manifested itself for all samples in the temperature range of 150 – 280°C and faded with increasing frequency. The peak intensity of ε values is proportional not only to the frequency, but also to the chromium concentration in the samples. The peak was most intense for the $x(Cr) = 0.7$ sample. We believe that the extremum in the dependence $\varepsilon(t)$ at 225°C may be due to water desorption. Due to the tendency of the samples to absorb moisture, samples freshly calcined at 300°C were studied. The temperature dependences of the permittivity and the dielectric loss tangent are shown in Fig. 5.

The frequency dependences of the dielectric permittivity and the dielectric loss tangent do not show features associated with the behavior of water (Fig. 5). The dielectric permittivity of the samples at low temperatures does not show a frequency dependence (up to 300°C). Above this temperature, the permittivity at low frequencies begins to increase, which is associated with the activation of ionic conductivity. At high frequencies, the values of ε coincide. Each sample has its own limiting frequency, and for a sample with $x = 0.7$ it is minimal and equals $6 \cdot 10^4$ Hz. Apparently, in the $x = 0.7$ sample, the largest contribution of ionic conductivity is manifested, this is also indicated by the observed values of the permittivity. From Fig. 5 we see that on a logarithmic scale, the dependence of the dielectric loss tangent tan δ on frequency is straight parallel lines. With the same scale on both axes, the angle of inclination will be 45°. Therefore, the product RC in the first approximation does not depend on the frequency. As Fig. 5 shows the sample capacity weakly dependent on the temperature and the frequency. Therefore, the change in temperature mainly affects the resistance of the resistor, which can be observed in Fig. S2 (supplementary material), which shows the dependence of the impedance modulus and the phase angle of the dehydrated samples. As Fig. S3 (supplementary material) shows, the effect of adsorbed water is significantly reduced for the dried samples. The impedance modulus is directly proportional to the frequency at temperatures below 225°C ($x = 0.7$), which indicates the flow of predominantly polarization currents. With increasing temperature, the frequency independence of the impedance modulus is observed, which is due to the activation of ion transport. The activation temperature is the lower, the higher the chromium content in the samples. As can be seen from Fig. S3 (supplementary material), a significant difference in the phase angle from 90 degrees and the frequency independence of the impedance modulus of anhydrous samples is observed at higher temperatures and is due to the activation of ionic conductivity. In particular, for sample $x = 0.7$ this temperature corresponds to 225°C, and for $x = 0.3$ it is equal to 300°C, confirming the thesis about the higher electrical conductivity of the sample with the highest chromium content.

The hodographs of the samples have the shape of an almost perfect semicircle. Therefore, the equivalent circuit of the sample will be a parallel RC — two-terminal network. Hodographs at lower temperatures have the shape of an arc, which is distorted by noise.

Calculation of the values of activation energy of conductivity in the samples showed that the lowest value is characterized by a sample with a high content of chromium ($x = 0.7$) 1.39 eV, for a sample with $x = 0.3$ the activation energy is 1.48 eV. High values of activation energy, more than 1 eV, can be associated with the activation of ionic conduction. As Fig. 6 shows, the through conductivity is the higher, the higher the content of chromium ions in the samples, which may be due to the formation of oxygen vacancies due to heterovalent substitution, as well as the tendency of chromium samples to absorb water. In general, the electrical properties of the sample are typical of dielectrics with

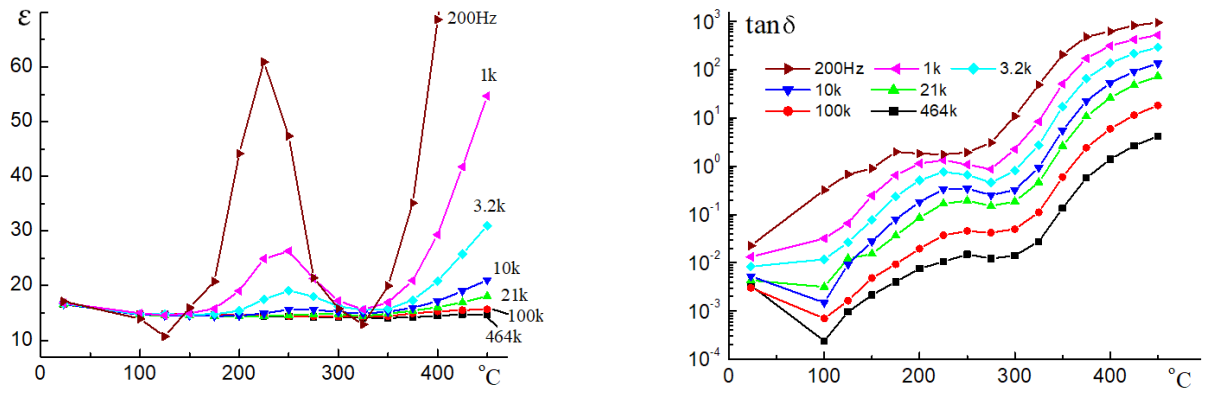

Fig. 4. (Color online) Dielectric permittivity and dielectric loss tangent (up to 450°C) for $Bi_2Mg_{0.3}Cr_{0.7}Ta_2O_{9.5-\Delta}$ samples stored in air.

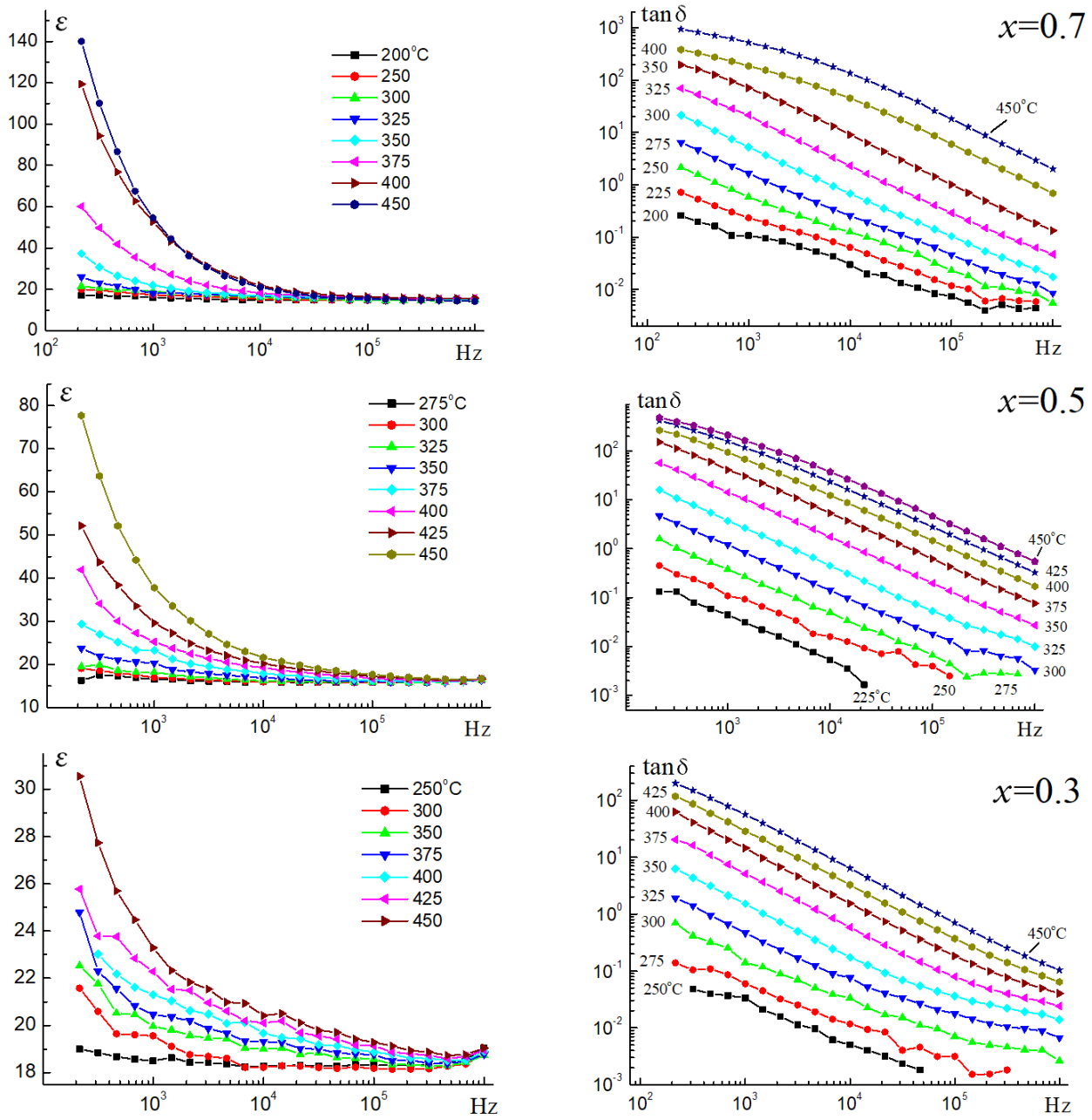

Fig. 5. (Color online) Dielectric permittivity and dielectric loss tangent (up to 450°C) for dehydrated $Bi_2Mg_{1-x}Cr_xTa_2O_{9.5-\Delta}$ samples.

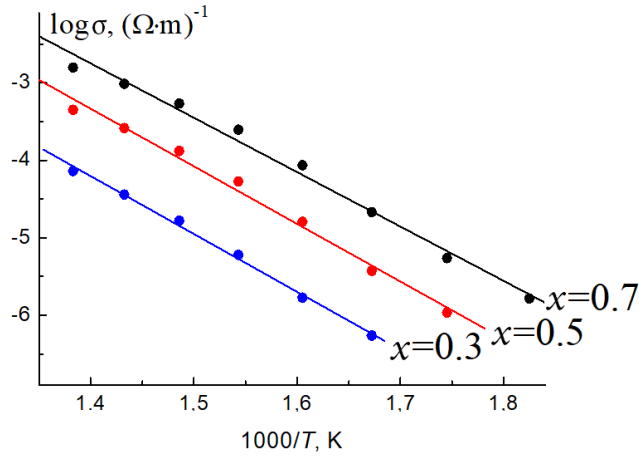

Fig. 6. (Color online) Temperature dependences of the specific conductivity of the $Bi_2Mg_{1-x}Cr_xTa_2O_{9.5-\Delta}$ samples plotted on the Arrhenius scale.

relatively high permittivity and low dielectric losses. When the sample is heated, the dielectric loss and permittivity in the low-frequency region increase, which may be due to the activation of oxygen anions.

4. Conclusions

The paper characterizes a series of $Bi_2Mg_{1-x}Cr_xTa_2O_{9.5-\Delta}$ solid solutions synthesized by the solid-phase method. The unit cell parameter obeys Vegard's rule. The microstructure of the samples is porous, dendrite-like. The samples are characterized by a significant reflection in the green (552 and 558 nm) region. A weak reflex is observed in the red (710 nm) range. The band gap for direct allowed transitions in $x(Cr) = 0.3$ and 0.7 samples is 1.52 and 1.58 nm and 2.29 and 2.14 eV, respectively. The electrical properties of the sample are typical of dielectrics with

relatively high permittivity and low dielectric losses. When the sample is heated, the dielectric loss and permittivity in the low-frequency region increase, which may be due to the activation of oxygen anions. Chromium pyrochlores have been found to be capable of adsorbing water.

Supplementary material. *The online version of this paper contains supplementary material available free of charge at the journal's website (lettersonmaterials.com).*

References

1. S. Murugesan, M.N. Huda, Y. Yan, M.M. Al-Jassim, V. Subramanian. J. Phys. Chem. C. 114, 10598 (2010). Crossref
2. C.C. Khaw, K.B. Tan, C.K. Lee. Ceram. Intern. 35, 1473 (2009). Crossref
3. G. Giampaoli, T. Siritanon, B. Day, J. Li, M. A. Subramanian. Prog. Solid State Chem. 50, 16 (2018). Crossref
4. J. Pandey, V. Shrivastava, R. Nagarajan. Inorg. Chem. 57, 13667 (2018). Crossref
5. M.A. Subramanian, G. Aravamudan, G.V. Subba Rao. Prog. Solid State Chem. 15, 55 (1983). Crossref
6. R.A. McCauley. J. Appl. Phys. 51, 290 (1980). Crossref
7. G.C. Miles, A.R. West. J. Am. Ceram. Soc. 89, 1042 (2006). Crossref
8. F. Matteucci, G. Cruciani, M. Dondi, G. Baldi, A. Barzanti. Acta Mater. 55, 2229 (2007). Crossref
9. D. Huiling, Y. Xi. Journal of Materials Science: Materials in Electronics. 15, 613 (2004). Crossref
10. N.A. Zhuk, M.G. Krzhizhanovskaya, A.V. Koroleva, S.V. Nekipelov, V.V. Kharton, N.A. Sekushin. Inorgan. Chem. 60, 4924 (2021). Crossref
11. N.A. Zhuk, M.G. Krzhizhanovskaya, A.V. Koroleva, A.A. Reveguk, D.V. Sivkov, S.V. Nekipelov. Ceram. Intern. 48, 14849 (2022). Crossref
12. N.A. Zhuk, M.G. Krzhizhanovskaya. Ceram. Int. 47, 30099 (2021). Crossref
13. N.A. Zhuk, M.G. Krzhizhanovskaya, A.V. Koroleva, S.V. Nekipelov, D.V. Sivkov, V.N. Sivkov, A.M. Lebedev, R.G. Chumakov, B.A. Makeev, V.V. Kharton, V.V. Panova, R.I. Korolev. Sol. St. Sci. 125, 106820 (2022). Crossref
14. N.A. Zhuk, N.A. Sekushin, V.G. Semenov, A.V. Fedorova, A.A. Selyutin, M.G. Krzhizhanovskaya, V.P. Lutoev, B.A. Makeev, V.V. Kharton, D.N. Sivkov, A.D. Shpynova. J. Alloys Comps. 903, 163928 (2022). Crossref
15. N.A. Zhuk, M.G. Krzhizhanovskaya, N.A. Sekushin, V.V. Kharton, A.V. Koroleva, S.V. Nekipelov, D.V. Sivkov, V.N. Sivkov, B.A. Makeev, A.M. Lebedev, R.G. Chumakov, S.Y. Kovalenko. ACS Omega. 6, 23262 (2021). Crossref
16. F.A. Jusoh, K.B. Tan, Z. Zainal, S.K. Chen, C.C. Khaw, O.J. Lee. J. Mater. Res. Techn. 9, 11022 (2020). Crossref
17. M.P. Chon, K.B. Tan, Z. Zainal, Y.H. Taufiq-Yap, P.Y. Tan, C.C. Khaw, S.K. Chen. J. Appl. Ceram. Techn. 13, 718 (2016). Crossref
18. M.P. Chon, K.B. Tan, C.C. Khaw, Z. Zainal, Y.H. Taufiq-Yap, S.K. Chen, P.Y. Tan. J. Alloys Comp. 675, 116 (2016). Crossref
19. C.C. Khaw, K.B. Tan, C.K. Lee, A.R. West. J. Eur. Ceram. Soc. 32, 671 (2012). Crossref
20. Ismunandar, T. Kamiyama, K. Oikawa, A. Hoshikawa, B.J. Kennedy, Y. Kubota, K. Kato. Mater. Res. Bull. 39, 553 (2004). Crossref
21. R.D. Shannon. Acta Crystallogr. A. 32, 751 (1976). Crossref
22. N.A. Zhuk, I.V. Piir, N.V. Chezhina. Russ. J. General Chem. 76, 1705 (2006). Crossref
23. N.A. Zhuk, I.V. Piir, A.L. Pimenov, N.V. Chezhina. Russ. J. General Chem. 77, 990 (2007). Crossref
24. N.A. Zhuk, M.G. Krzhizhanovskaya, N.A. Sekushin, V.V. Kharton, B.A. Makeev, V.A. Belyy, R.I. Korolev. Ceram. Intern. 47, 19424 (2021). Crossref